Chapter 2

Analytical Modeling of Channel Potential and Threshold Voltage of DG-JLFETs with a Vertical Gaussian-Like Doping Profile

2.1 Introduction

It has already been discussed in Chapter-1 that the JLFETs have many advantages such as better scalability [Colinge *et al.*(2010)], higher carrier speed [Colinge *et al.*(2010)], large drain current [Chiang (2012)], and better features for RF analog [Doria *et al.*(2011)] and digital memory [Choi *et al.* (2011)] circuits and systems applications over the conventional inversion mode MOSFETs. The fundamental working and device physics of the JLFETs [Colinge et al.(2010), Lee *et al.*(2009), Chiang (2012), Colinge *et al.(*2011), Lee *et al.*(2011)] have also been discussed in Chapter-1. Due to better scalability and smaller SCEs of the double-gate (DG) MOS transistors over the single gate MOS structures, a number of researchers have investigated the characteristics of the short-channel DG-JLFETs [Gnani *et al.*(2012), Jin *et al.* (2012), Holtij *et al.(*2014), Gnudi *et al*.(2013), Kumari *et al*.(2015)] with a uniformly doped channel as discussed in details in Chapter-1. Recently, Mondal *et al.* [Mondal *et al.*(2013), Mondal *et al.*(2015)] have investigated through TCAD simulation that a vertical Gaussian doping profile in the channel can be used to improve the subthreshold characteristics of the JL SOI-FETs [Mondal *et al.*(2013)] and JL-FinFETs [Mondal *et al.*(2015)]. Since there is no

theoretical model for the subthreshold characteristics of the DG JLFETs with a non-uniform channel profile, we have made an attempt in the present chapter to develop the analytical models for the 2D channel potential function and threshold voltage characteristics of the short-channel DG JLFETs with a vertical Gaussian-like doping profile in the channel. The actual non-analytic Gaussian function considered by [Mondal *et al.*(2015)] has been replaced by a Gaussian-like function originally proposed by Dasgupta and Lahiri [Dasgupta and Lahiri (1986)] for the simplification of analysis as discussed in Chapter-1. The layout of the present chapter is given as follows:

In this chapter, the 2D Poisson equation has been solved for the DG-JLFETs with a vertical Gaussian-like doping profile to analytically model the channel potential and threshold voltage of the device. The theoretical model derivation of the 2D channel potential function obtained by solving the 2D Poisson's equation using Evanescent mode analysis method is discussed in Sec.2.2.1. The position of the conduction path in the channel has been derived in Sec.2.2.2 for modeling the threshold voltage of the DG JLFETs in Sec.2.2.3. The results and discussion have been discussed in Sec. 2.3. Finally, Sec. 2.4 includes the conclusion of the present chapter.

2.2 Model Derivation

2.2.1 Channel Potential

The schematic view of DG-JLFET structure considered in the present study is shown in Fig.2.1 where, t_{si}, L, and t_{ox} are the channel thickness, channel length, and gate oxide

thickness, with V_{gs} and V_{ds} as the gate-to-source and drain-to-source voltages respectively. For simplicity, the source and drain regions located at the left and right sides of the highly doped bulk silicon channel are assumed to be of zero thickness as considered by T.K. Chiang [Chiang (2012)]. The x and y-axes are considered along with the silicon thickness and source-channel interface respectively. The image of the simulated structure is shown in Fig.2.2. The Gaussian-like doping profile [Dubey *et al.*(2010)] in the channel is assumed perpendicular to the gate oxide and in the x direction as shown in Fig. 2.1 and 2.2.

Let the Gaussian-like doping profile in the vertical direction of the channel be $N_{GL}(x)$ which is expressed as [Dubey *et al.*(2010), Dasgupta and Lahiri (1986)]

$$N_{GL}(x) = cN_{pk}\left((a+2b\alpha X)^2 - 2b\right)\exp(-a\alpha X - bX^2) \tag{2.1}$$

where $a = 1.786$, $b = 0.646$ and $c = 0.56$ are fitting parameters; $\alpha = +1$ for $x > 0$ and $\alpha = -1$ for $x < 0$; $X = \dfrac{x - R_p}{\sqrt{2}\sigma_p}$ where R_p is the projected range and σ_p is the straggle of the Gaussian doping profile, and N_{pk} is the peak doping at $x = R_p$.

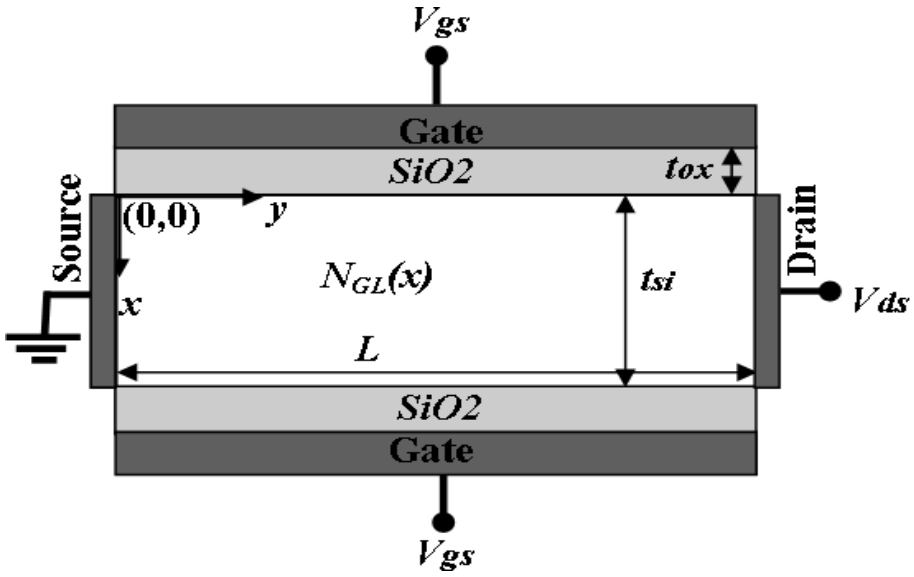

Fig. 2.1: Simplified two-dimensional schematic view of DG- JLFET.

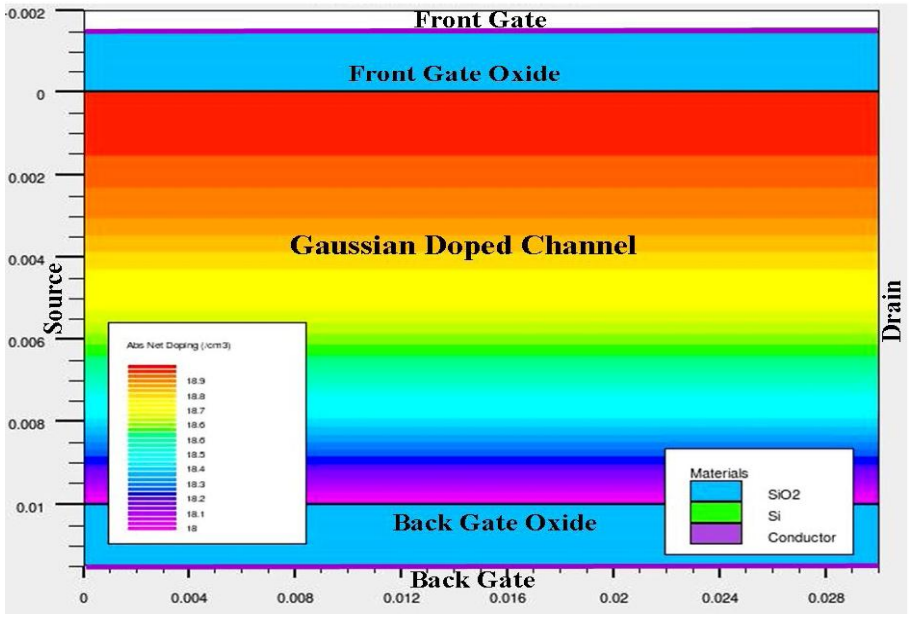

Fig. 2.2: The simulated view of Gaussian doped DG-JLFET.

The two-dimensional channel potential, say $\psi(x,y)$, can be calculated by solving the following 2D Poisson's equation

$$\frac{\partial^2\psi(x,y)}{\partial x^2}+\frac{\partial^2\psi(x,y)}{\partial y^2}=-\frac{q}{\varepsilon_{si}}N_{GL}(x) \tag{2.2}$$

The boundary conditions used for solving Eq. (2.2) are given by [Jin *et al.*(2012),Dubey *et al.*(2010)]

$$V_{gs}-V_{ff}-\psi(0,y)=-\frac{\varepsilon_{si}}{C_{ox}}\frac{\partial\psi(x,y)}{\partial x}\bigg|_{x=0} \tag{2.3}$$

$$V_{gs}-V_{bf}-\psi(t_{si},y)=\frac{\varepsilon_{si}}{C_{ox}}\frac{\partial\psi(x,y)}{\partial x}\bigg|_{x=t_{si}} \tag{2.4}$$

$$\psi(x,0)=V_{bi}(x) \tag{2.5}$$

$$\psi(x,L)=V_{bi}(x)+V_{ds} \tag{2.6}$$

where V_{ff} and V_{bf} are the flat band voltages of the front and back silicon/oxide interfaces with respect to intrinsic Fermi level; ε_{si} and ε_{ox} are the permittivities of the silicon and SiO_2 respectively, t_{ox} is the oxide thickness, $C_{ox}=\frac{\varepsilon_{ox}}{t_{ox}}$ is the gate oxide capacitance and $V_{bi}(x)$ is the Fermi potential obtained after including bandgap narrowing phenomenon which is given in Eq. (2.8), Since the channel region is heavily doped, there may be a change in the energy band gap, intrinsic carrier concentration and electron affinity of the Si in the channel due to the band-gap narrowing phenomenon

[Kumari *et al*.(2015)]. To incorporate the band gap narrowing phenomenon in the present model, the change in the energy band gap, effective intrinsic carrier concentration and effective electron affinity of the Si under heavily doped conditions can respectively be described as [Slotboom and Graaff(1976), Slotboom and Graaff (1977)]

$$n_{ieff} = \sqrt{n_i^{\,2} \exp\left(\frac{\Delta E_g}{kT}\right)} \quad \text{and} \quad \chi_{eff} = \chi + 0.5(\Delta E_g) \tag{2.7}$$

$$V_{bi}(x) = V_T \ln\left(\frac{N_{GL}(x)}{n_{ieff}}\right) \tag{2.8}$$

$$\Delta E_g = BGN.E\left\{\ln\left(\frac{N_{GL}(x)}{BGN.N}\right) + \left[\ln\left(\frac{N_{GL}(x)}{BGN.N}\right)^2 + BGN.C\right]^{\frac{1}{2}}\right\} \tag{2.9}$$

$$\text{and } E_{geff} = E_g - \Delta E_g \tag{2.10}$$

where, $BGN.E = 9.0\times10^{-3}\text{eV}$, $BGN.N = 1.0\times10^{17}\,\text{cm}^{-3}$, and $BGN.C = 0.5$ are some empirical constants; n_i is the intrinsic carrier concentration of Si, n_{ieff} is the effective intrinsic concentration, χ_{eff} is the effective electron affinity, χ is the electron affinity and V_T is the thermal voltage.

Using the Evanescent-mode analysis, the solution of Eq. (2.2) for the 2D potential function $\psi(x, y)$ can be written as [Chen *et al.* (2002) Dubey *et al.*(2010)]

$$\psi(x, y) = U(x) + V(x, y) \tag{2.11}$$

where, $U(x)$ is the 1D potential function responsible for the long-channel device characteristics to be obtained by solving the following 1D Poisson's equation:

$$\frac{d^2U(x)}{dx^2} = -\frac{q}{\varepsilon_{si}} N_{GL}(x) \tag{2.12}$$

and $V(x,y)$ the 2D potential function responsible for the short-channel effects of the device to be obtained by solving the following 2D Laplace equation:

$$\frac{\partial^2 V(x,y)}{\partial x^2} + \frac{\partial^2 V(x,y)}{\partial y^2} = 0 \tag{2.13}$$

The general solution of Eq. (2.12) can be given by

$$U(x) = -\frac{qx_b^{\,2}}{\varepsilon_{si}}\left[cN_{pk}\exp\left(-a\alpha X - bX^2\right) + AX + B\right] \tag{2.14}$$

where, A and B are constants which can be calculated by using the following boundary conditions:

$$V_{gs} - V_{ff} - U(0) = -\frac{\varepsilon_{si}}{C_{ox}}\frac{\partial U(x,y)}{\partial x}\bigg|_{x=0} \tag{2.15}$$

$$V_{gs} - V_{fb} - U(t_{si}) = \frac{\varepsilon_{si}}{C_{ox}}\frac{\partial U(x,y)}{\partial x}\bigg|_{x=t_{si}} \tag{2.16}$$

From Eqs. (2.15) and (2.16), A and B can be written as

$$A = \frac{\left(V_{bef} - V_{fef}\right) - \frac{qx_b^{\,2}}{\varepsilon_{si}}(E_f - E_b) - \frac{qx_b}{C_{ox}}(E_{df} + E_{db})}{\frac{qx_b^{\,2}}{\varepsilon_{si}}(X_f - X_b) - \frac{2qx_b}{C_{ox}}} \tag{2.17}$$

$$B = -\frac{\varepsilon_{si}}{2C_{ox}qx_b{}^2}\left[(V_{fef}+V_{bef})+\frac{qx_b}{C_{ox}}(E_{df}-E_{db})+\frac{qx_b{}^2}{\varepsilon_{si}}(E_f+E_b)+C_{ox}\frac{qx_b{}^2}{\varepsilon_{si}}A(X_f+X_b)\right] \quad (2.18)$$

where, $V_{ff} = V_{fb} = \frac{1}{q}(\phi_m - \chi e_{ff} - \frac{E_{geff}}{2})$ (2.19)

and ϕ_m is the metal gate work function in eV,

$$V_{fef} = V_{gs} - V_{ff} \quad (2.20)$$

$$V_{bef} = V_{gs} - V_{fb} \quad (2.21)$$

$$X_f = X|_{x=o} = -\frac{R_p}{x_b} \quad (2.22)$$

$$X_b = X|_{x=t_{si}} = \frac{t_{si} - R_p}{x_b} \quad (2.23)$$

$$E_f = cN_{pk}\exp(-aX_f - bX_f{}^2) \quad (2.24)$$

$$E_b = cN_{pk}\exp(-aX_b - bX_b{}^2) \quad (2.25)$$

$$E_{df} = cN_{pk}(a+2bX_f)\exp(-aX_f - bX_f{}^2) \quad (2.26)$$

$$E_{db} = cN_{pk}(a+2bX_b)\exp(-aX_b - bX_b{}^2) \quad (2.27)$$

To obtain $V(x,y)$ by solving Eq.(2.13), we can use the following boundary conditions [Dubey *et al.*(2010)]

$$V(x,y)|_{x=0} = -\frac{\varepsilon_{si}}{C_{ox}}\left.\frac{\partial V(x,y)}{\partial x}\right|_{x=0} \quad (2.28)$$

$$V(x,y)\big|_{x=t_{si}} = \frac{\varepsilon_{si}}{C_{ox}} \frac{\partial V(x,y)}{\partial x}\bigg|_{x=t_{si}} \tag{2.29}$$

$$V(x,0) = V_{bi}(x) - U(x) \tag{2.30}$$

$$V(x,L) = V_{bi}(x) + V_{ds} - U(x) \tag{2.31}$$

The general solution of Eq. (2.13) can be expressed as [Dubey et al.(2010)]

$$V(x,y) = \sum_{n=1}^{\infty} \frac{\cos(\eta x)}{\sinh(\eta L)} \left[V_n \sinh(\eta L - \eta y) + V_n' \sinh(\eta y) \right] \tag{2.32}$$

where, $\eta = \frac{\pi}{\lambda}$ with $\lambda = \left[t_{si} + \frac{2\varepsilon_{si} t_{ox}}{\varepsilon_{ox}} \right]$ [Frank *et al.* (1998), Monroe *et al.* (1998)] and,

V_n and V_n' are arbitrary constants.

Following the methodology of Dubey *et al.*(2010), $V(x,y)$ can be approximated by holding only the lowest-order value, i.e. $n=1$ and can be expressed as

$$V(x,y) \approx \frac{\cos(\eta x)}{\sinh(\eta L)} \left[V_1 \sinh(\eta L - \eta y) + V_1' \sinh(\eta y) \right] \tag{2.33}$$

where, V_1 and V_1' are the fourier constants which can be obtained by solving the boundary conditions described by Eqs. (2.28), (2.29), (2.30) and (2.31) as

$$V_1 = 4\left[2t_{si} + \eta^{-1} \sin(2\eta t_{si}) \right]^{-1} \left[K_1 \eta^{-1} \sin(\eta t_{si}) - K_2 \right] \tag{2.34}$$

$$V_1' = 4\left[2t_{si} + \eta^{-1} \sin(2\eta t_{si}) \right]^{-1} \left[(K_1 + V_{ds}) \eta^{-1} \sin(\eta t_{si}) - K_2 \right] \tag{2.35}$$

where, the constants K_1 and K_2 are given by

$$K_1 = V_T \ln\left(\frac{N_{pk}}{n_i}\right) + \left[\frac{qx_b^{\,2}}{\varepsilon_{si}} B + cN_{pk}\frac{qx_b^{\,2}}{\varepsilon_{si}}\right] \tag{2.36}$$

and $K_2 = Z_1 + Z_2$ (2.37)

where, $Z_1 = -\frac{K_4}{x_b}(K_3 a - \frac{qx_b^{\,2}}{\varepsilon_{si}} A)(\eta t_{si} - \eta R_p + \cot(\eta t_{si}) - \mathrm{cosec}(\eta t_{si}))$ (2.38)

$$Z_2 = -\frac{bK_3K_4}{x_b^{\,2}}(\eta(t_{si} - R_p)^2 + 2(t_{si} - R_p)\cot(\eta t_{si}) + 2R_p\,\mathrm{cosec}(\eta t_{si}) - 2\eta^{-1}) \tag{2.39}$$

$$K_3 = \frac{cqN_{pk}x_b^{\,2}}{\varepsilon_{si}} \tag{2.40}$$

and $K_4 = \frac{\sin(\eta t_{si})}{\eta^2}$ (2.41)

The minimum potential at the conduction path is very important since it determines the threshold voltage from Eq. (2.11), we can write

$$\psi_{\min}(x) = \psi(x,y)\big|_{y=y_{\min}} = U(x) + V(x, y_{\min}) \tag{2.42}$$

where, $y_{\min}$ is the position along the channel where

$$\left.\frac{\partial\psi(x,y)}{\partial y}\right|_{y=y_{\min}} = 0 \tag{2.43}$$

Assuming $\eta L >> 1$ for the practical devices, Eq. (2.43) gives

$$y_{\min} = \frac{L}{2} + \frac{\ln\left[\sqrt{\frac{V_1}{V_1'}}\right]}{\eta} \tag{2.44}$$

From Eq. (2.42) and (2.44), we can write

$$\psi_{\min}(x) \approx U(x) + 2\cos(\eta x)\sqrt{V_1 V_1'}\exp\left(-\frac{\eta L}{2}\right) \tag{2.45}$$

2.2.2 Conduction Path Potential

The effective conduction path in the channel is defined as the location $x = x_C$ where the minimum potential function $\psi_{\min}(x)$ has the maximum value [Dey *et al.* (2008)]. Thus, we can write

$$\left.\frac{d\psi_{\min}(x)}{dx}\right|_{x=x_C} = 0 \tag{2.46}$$

Using Eq. (2.45) in Eq. (2.46) and after simplification we can obtain

$$Q_0 x_c^3 + Q_1 x_c^2 + Q_2 x_C - S_6 = 0 \tag{2.47}$$

where, $Q_0 = bS_4$, (2.48)

$$Q_1 = bS_2 + ax_b \alpha S_4 - 2bS_4 R_p \tag{2.49}$$

$$Q_2 = a\alpha x_b S_2 + bS_4 {R_p}^2 + S_3 {x_b}^2 - 2bS_2 R_p - {x_b}^2 S_4 - a\alpha x_b R_p S_4 \tag{2.50}$$

$$S_1 = \frac{V_1 \sinh(\eta(L - y_{\min})) + V_1' \sinh(\eta y_{\min})}{\sinh(\eta L)} \tag{2.51}$$

$$S_2 = cN_{pk}\left(a\alpha x_b - 2bR_p\right) \tag{2.52}$$

$$S_3 = \frac{\eta^2 \varepsilon_{si} S_1}{q}, \tag{2.53}$$

$$S_4 = 2cbN_{pk}, \tag{3.54}$$

$$S_5 = S_2 {x_b}^2 + S_2 a\alpha x_b R_p - bS_2 {R_p}^2 \tag{2.55}$$

and $S_6 = S_5 - A{x_b}^3$ (2.56)

The determinant (Δ) [Irving and Integers (2004)] of Eq. (2.47) is less than zero, so the Eq. (2.47) has one real root and two non-real complex conjugate roots.

where,

$$\Delta = 4Q_1^3 S_6 - 18Q_0 Q_1 Q_2 S_6 + Q_1^2 Q_2^2 - 4Q_0 Q_2^3 - 27Q_0^2 S_6^2 \tag{2.57}$$

Considering the real root of Eq. (3.46), the conduction path location $x = x_C$ can be given by [Irving *et al.*(2004)]

$$x_C = -\left[\frac{Q_1 + S_7 + (S_8/S_7)}{3Q_0}\right] \tag{2.58}$$

where, $S_7 = \sqrt[3]{\frac{S_9 + \sqrt{S_9^2 - 4S_8^3}}{2}}$ (2.59)

$$S_8 = Q_1^2 - 3Q_0 Q_2 \tag{2.60}$$

and $S_9 = 2Q_1^3 - 9Q_0 Q_1 Q_2 - 27Q_0^2 S_6$ (2.61)

2.2.3 Threshold Voltage Model

The threshold voltage of the JLFETs is the gate voltage which converts the fully depleted channel into a partially depleted one to start the bulk current conduction between the source and the drain of the device [Colinge *et al.* (2011)]. In other words,

the threshold voltage is the gate voltage at which the minimum channel potential $\psi_{\min}(x_C)$ at the bulk conduction path $x = x_C$ (where the vertical electric field becomes zero) equals to the Fermi potential $V_{bi}(x_C)$ when the flat band voltage is measured with respect to the intrinsic bulk Fermi level [Gnudi *et al.* (2013)]. Thus, we can write

$$\psi_{\min}(x_C)\big|_{V_{gs}=V_{th}} = V_{bi}(x_C) \tag{2.62}$$

which gives

$$V_{th} = V_{bi}(x_C) + T_1 + T_2 + \frac{qx_b{}^2 T_3}{\varepsilon_{si}} + \frac{V_{ff} + V_{fb}}{2} - V(x_C, y_{\min}) \tag{2.63}$$

$$\text{where, } T_1 = \frac{cqN_{pk}x_b{}^2 \exp(-a\alpha X - bX^2)}{\varepsilon_{si}}, \tag{2.64}$$

$$T_2 = \frac{qx_b{}^2 X}{\varepsilon_{si}}\left[\frac{-qx_b{}^2 C_{ox}(E_f - E_b) - qx_b(E_{df} + E_{db})}{\varepsilon_{si}S_2} + \frac{C_{ox}(V_{ff} - V_{fb})}{S_2}\right] \tag{2.65}$$

$$T_3 = -\left(2qx_b{}^2 C_{ox}\right)^{-1} \times \left[qx_b\varepsilon_{si}(E_{df} - E_{db}) + qx_b{}^2 C_{ox}(E_f + E_b) + qx_b{}^2 AC_{ox}(X_f + X_b)\right] \tag{2.66}$$

"Note that the threshold voltage is expected to decrease a little with the reduction in the Fermi potential $V_{bi}(x_C)$ owing to band-gap narrowing phenomenon as shown by Eq. (2.8)."

2.3 Results and Discussion

This section presents the potential distribution profile and the threshold voltage of the DG- JLFET with a vertical Gaussian-like doping profile, calculated from the proposed model. These model results are validated by comparing them with the ATLAS™ based 2D device simulation data which considers vertical Gaussian doping profile in channel

region instead of Gaussian-like doping. Chapter 1 mentions that Gaussian-like function shows a close resemblance to Gaussian functions and could be integrated twice over any finite interval. Thus, a match between simulation data and model results will not only validate the proposed model but also assure the proximity of Gaussian-like function with the Gaussian distribution function.

The values of different parameters used for simulation and computations are: $W.F = 5.1eV$, $t_{si} = 10nm, t_{ox} = 1.5nm$, and $N_{pk} = 1\times10^{19} cm^{-3}$. The 2D numerical simulations have been carried out in the similar manner as in Ref. [Mondal *et al.*(2013)] by using the *conmob*, *fldmob*, *prpmob*, *consrh*, *auger* and *bgn* models. The *conmob*, *fldmob* and *prpmob* models have been introduced for the concentration, lateral electric field and perpendicular electric field dependent mobility respectively. The *consrh* accounts for the Shockley–Read–Hall recombination with concentration dependent lifetime. Similarly, the Auger recombination occurring at high carrier density is introduced by applying *auger* model. Finally, *bgn* model is for the bandgap-narrowing to incorporate the effect due to high doping concentration in the channel. Further, the channel thickness is assumed to be greater than 7nm in the present study to neglect the quantum mechanical effects on the device characteristics [Choi *et al.*(2011)] for the simplification of the model.

To calibrate the simulation results and ensure the fabrication feasibility of the device under study, the ATLAS^{TM} TCAD simulation data for the drain current has been first compared with the experimental results for non-planar Silicon- on-Insulator Junctionless Transistor (SOI-JLT) reported in ref [Colinge *et al.* (2010)]. The reasonable good

matching ensures the validity of the simulation model used in this study.

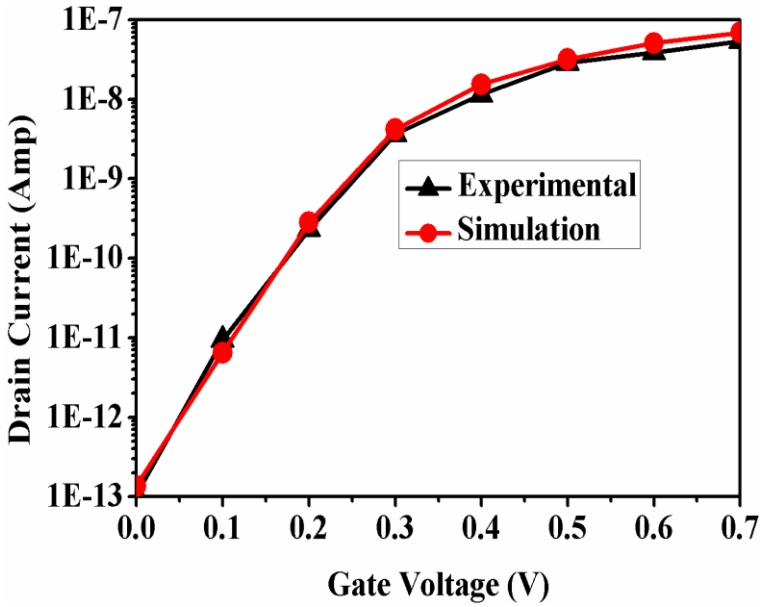

Fig.2.3: Simulation model calibration against non-planar JLFET experimental $I_{DS}-V_{GS}$ data from [Colinge *et al.* (2010)].

The threshold voltage has been computed in the ATLAS simulation by using the constant current method [Jeon *et al.* (2013)]. According to this method, the threshold voltage has been defined as the gate voltage at which the drain current $I_{DS}=10^{-7}(W/L)$[Jeon *et al.* (2013)] where, $W=1\mu m$ has been assumed as the channel width and L is channel length.

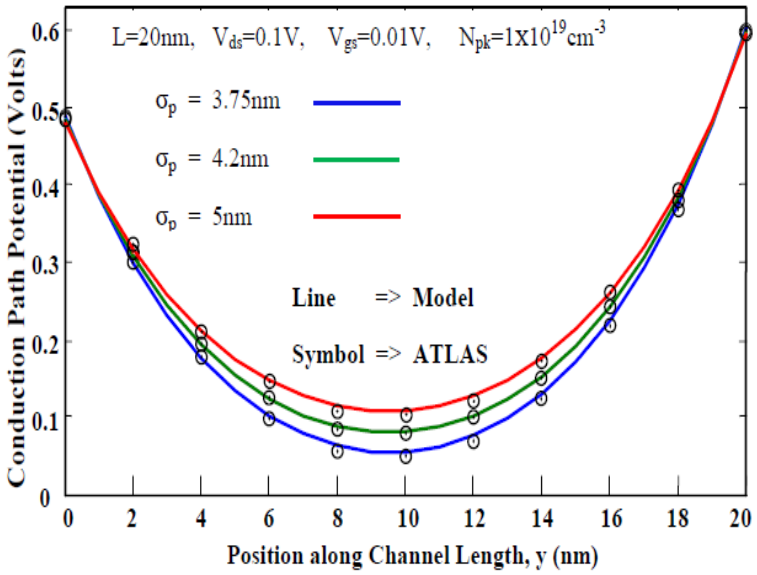

Fig.2.4: Conduction path potential variation along channel length for various straggle.

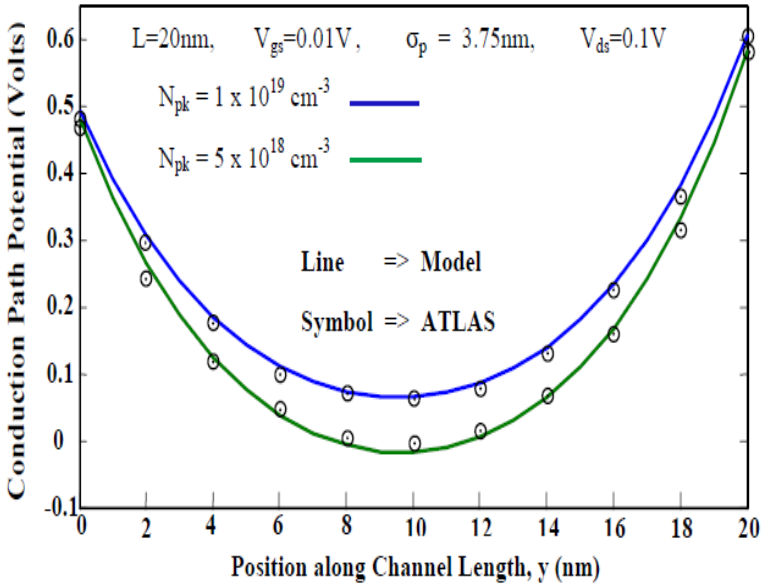

Fig.2.5: Conduction path potential variation along channel length for various doping concentration.

Fig.2.4 shows the potential at the conduction path as a function of position in the channel for different straggle parameter (σ_p) values of Gaussian-like doping profile and

compares the model result with simulation data. The increase in the minimum potential with σ_p implies a decrease in the barrier potential between the source and the channel.

In the channel region, the effect of a change in peak doping concentration on the conduction path potential can be easily distinguished from Fig.2.5. The variation of conduction path potential for two values of peak doping concentration demonstrates that the degradation of the source-channel barrier potential due to SCEs and DIBL can be compensated by increasing the doping concentration in the channel. Thus, a lightly doped JLFET is preferred for reduction in SCEs. However, excessively heavy doping introduces scattering issues, thereby degrading device characteristics.

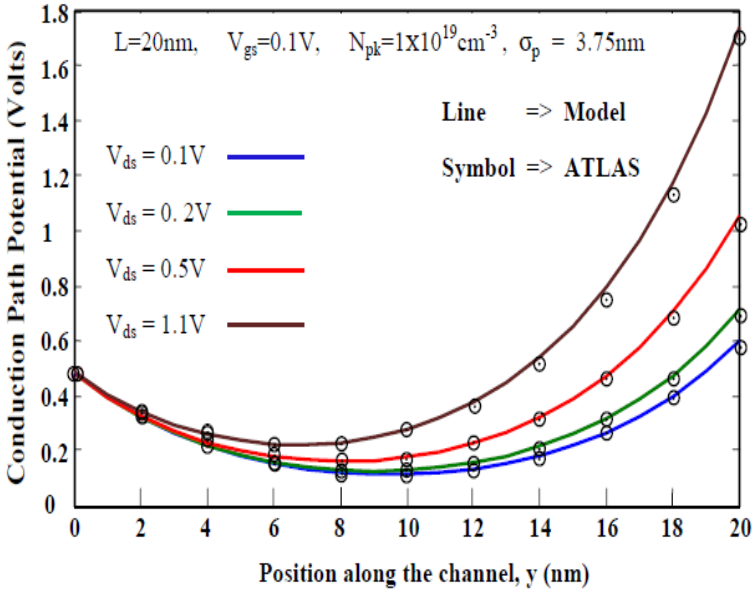

Fig.2.6: Conduction path potential variation for short channel length at different drain voltages.

The variations of conduction path potential along the channel for gate lengths of 20 nm and 60nm have been shown in Fig.2.6 and Fig.2.7 respectively for different drain-source voltages (V_{ds}). In Fig.2.6, there is a significant reduction in the source-channel potential barrier with the increased drain-source voltage for 20 nm gate length owing to the dominance of DIBL phenomenon at short channel length. For longer channel length of 60nm, the potential barrier for the same device remains almost unaffected by V_{ds} as shown in Fig.2.7. Thus, at long channel length, the DIBL effect is alleviated for the device. The proximity of the data extracted from both the simulation and model is discernible in Fig.2.6 and Fig.2.7 which precisely validates the proposed model.

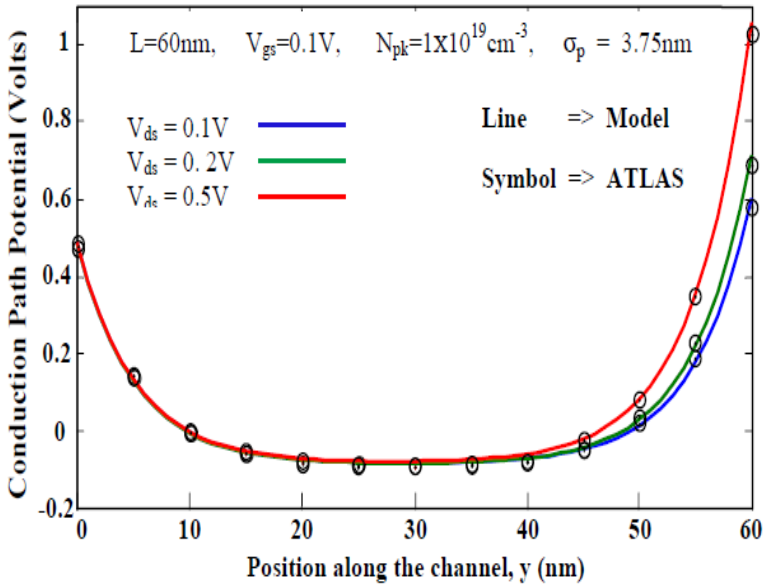

Fig.2.7: Conduction path potential variation for long channel length at different drain voltages.

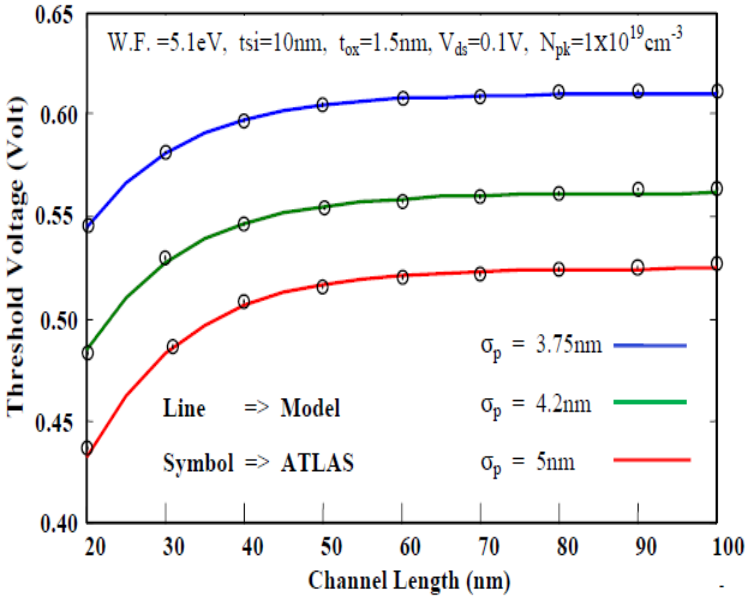

Fig.2.8: Threshold voltage variation with channel length for different straggle.

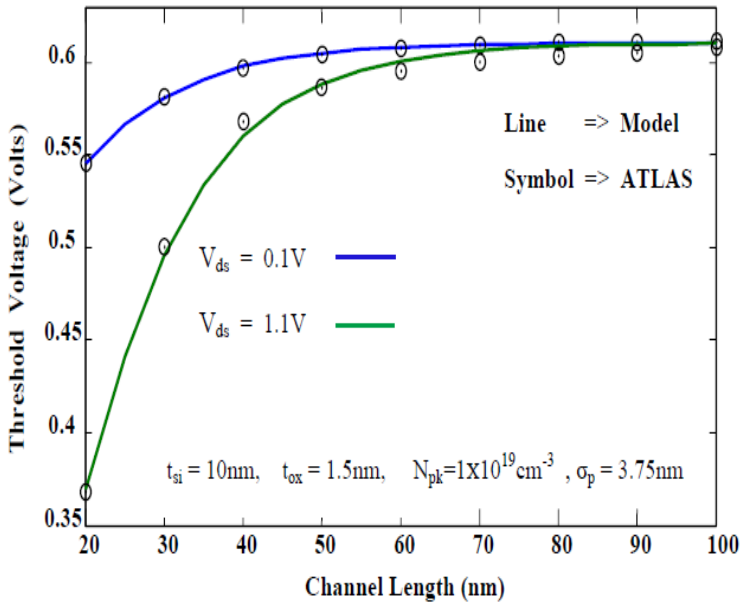

Fig.2.9: Threshold voltage variation with channel length for different drain voltages.

The influence of straggle parameter, σ_p on the threshold voltage variation as a function of channel length, has been demonstrated in Fig.2.8. The increase in threshold voltage with the decrease in σ_p is a consequence of the increase in the source-channel potential barrier as discussed earlier. It is also observed that the degradation of the threshold voltage due to SCEs starts to dominate, for gate lengths below $\approx 60nm$. Moreover, the reduction in straggle parameter not only offers a remarkable increase in the threshold voltage but also contributes in diminution of threshold voltage roll-off as channel length reduces below $\approx 60nm$. Thus, the straggle parameter σ_p can be used for improving SCEs and further optimizing the subthreshold performance.

Fig.2.9 presents the threshold voltage variation as a function of channel length for two values of drain voltages, $V_{ds} = 0.1\,\text{V}$ and $V_{ds} = 1.1\,\text{V}$. The threshold voltage is decreased rapidly with the increase in V_{ds} for channel lengths below ~60nm due to the increase in the DIBL and SCEs. For longer channel lengths (> 60nm), it becomes almost independent of V_{ds} due to negligible DIBL phenomenon.

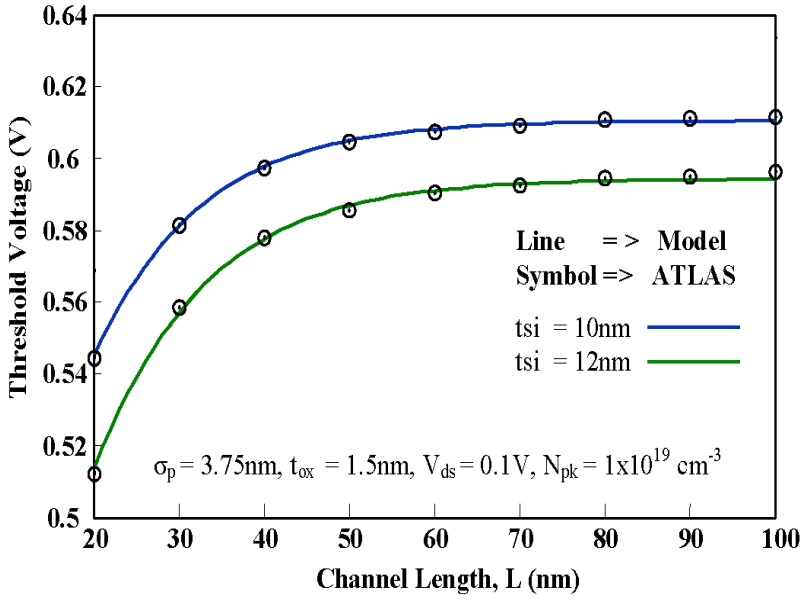

Fig.2.10: Threshold voltage variation with channel length for different silicon thicknesses (t_{si}).

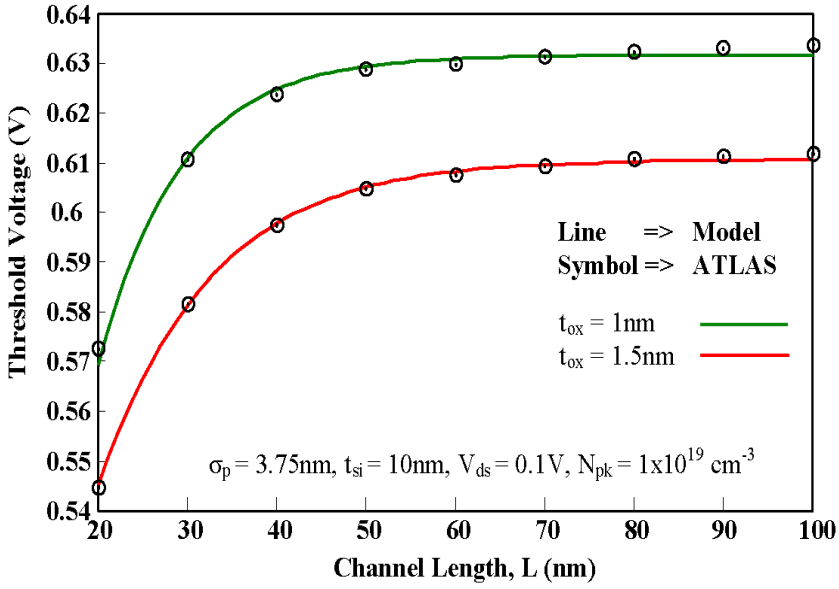

Fig.2.11: Threshold voltage variation with channel length for different oxide thicknesses.

The effects of silicon channel thickness (t_{si}) and oxide thickness (t_{ox}) on the threshold voltage have been demonstrated in Fig.2.10 and Fig.2.11, respectively. It is observed that the threshold voltage is increased with the decrease in t_{si} as well as t_{ox}. In other words, the control of gate on the channel is reduced with the increased values of t_{si} and t_{ox}. These results show that the subthreshold current will be increased with the increase in t_{si} and t_{ox} as reported by other researchers [Jin *et al.*(2012)].

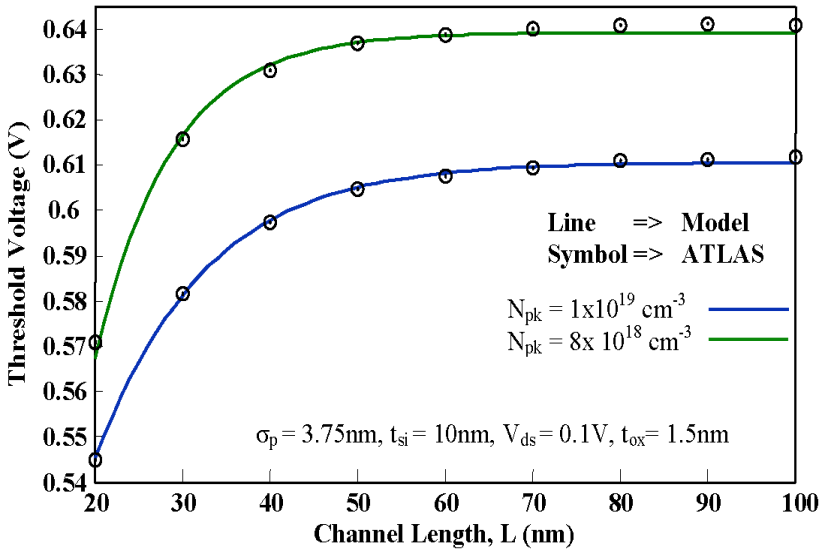

Fig.2.12: Threshold voltage variation with channel length for different peak doping concentrations.

The effect of peak doping concentration (N_{pk}) of the Gaussian profile on the threshold voltage has been shown in Fig.2.12. The increase in peak doping concentration of the Gaussian profile increases the average doping concentration in the channel which, in turn, decreases the threshold voltage. Note that observations are in coherence with the increase in the source-channel potential with N_{pk} as demonstrated earlier against the

observations in Fig.2.5. As N_{pk} decreases from $1\times10^{19}\,\text{cm}^{-3}$ to $8\times10^{18}\,\text{cm}^{-3}$, threshold voltage increases from 0.545V to 0.57V at 20 nm channel length and from 0.61V to 0.64V at 100nm. The N_{pk} can be used to compensate the degradation of the threshold voltage due to the SCEs and DIBL.

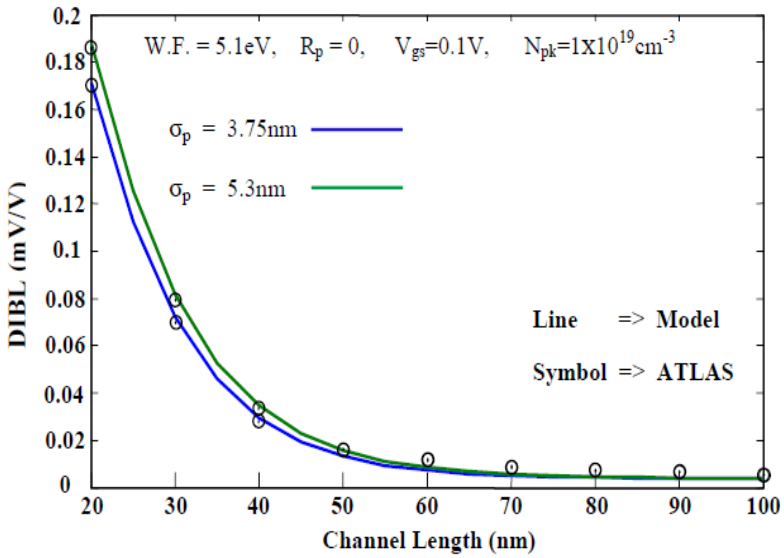

Fig.2.13: DIBL variation with channel length for different straggle.

Finally, to investigate the effects of σ_p and channel lengths on DIBL of the device, we have plotted the DIBL as a function of channel length in Fig.2.13 for two values of σ_p where the DIBL has been quantified by

$$DIBL = \frac{V_{th}|V_{ds}=0.1\text{V} - V_{th}|V_{ds}=1.1\text{V}}{\left(V_{ds}=1.1V\right)-\left(V_{ds}=0.1V\right)} \tag{2.67}$$

It may be noted that the DIBL at ~20nm channel length increases from ~170mV/V to ~185mV/V when σ_p is increased from 3.75nm to 5.3nm. However, the DIBL becomes

almost insensitive to σ_p for channel lengths above 60nm. The close matching of the model results with the ATLAS simulation data in all the figures shows the validity of the model proposed in this chapter.

2.4 Conclusion

In this chapter, a new analytical model for the channel potential and threshold voltage of DG-JLFET structure with a vertical Gaussian-like doping profile in the channel has been proposed. The 2D Poisson's equation has been solved by the superposition method. The 2D channel potential has been assumed to be the summation of the potential of the conventional long-channel device obtained by solving 1D Poisson equation and 2D potential function obtained by solving the 2D Laplace equation. The potential function has then been used to model the threshold voltage of the device. The analytical model results have been compared with the ATLAS^{TM} based 2D simulation data for verifying the validity of the proposed model. For devices with gate lengths below ~60nm, the source-channel potential barrier as well as threshold voltage is observed to be decreased with the decrease in the channel length and peak doping of the Gaussian profile, and with the increase in the drain-source voltage, silicon channel thickness, gate oxide thickness and straggle parameter of the Gaussian profile in the channel. It is observed that the straggle parameter of the channel profile can be used as an extra parameter in addition to the peak doping concentration of the channel profile for the optimization of the DIBL and SCEs in the device.